Magnetized Fiber Orientation Control in Solidifying Composites: Numerical Simulation

G. S. Dulikravich

B. Kosovic

Department of Aerospace Engineering,
The Pennsylvania State University,
University Park, PA 16802

S. Lee

Agency for Defense Development,
Taejon, Republic of Korea

This work deals with the development of a numerical algorithm for the prediction of magnetic force lines inside a flowing solidifying melt with the ultimate purpose of simulating and controlling alignment of short nickel-coated fibers during the curing process in composites. A complete mathematical model and an accompanying computer program have been developed for the simulation of a steady laminar flow of an incompressible fluid with strong heat transfer (involving solidification) and a strong superimposed magnetic field. An extended form of the Boussinesq approximation allowing for temperature-dependent physical properties of the fluid and the solid including latent heat of phase change was incorporated. This formulation simultaneously predicts detailed velocity, pressure, and temperature fields in the moving fluid while capturing the forming solid phase by using a single computer code. The same code can simulate the reverse process of thawing or melting of the solid phase. The computed sample configurations involve a two-dimensional closed container, a straight and a U-shaped channel, and a passage of an arbitrary shape. It was found that the presence of an external steady magnetic field: (a) diminishes flow field vorticity, (b) causes higher velocity gradients within the boundary layers, (c) is able to orient magnetized fibers along the lines of local magnetic lines of forces.

Introduction

It is well known that the defects in short fiber composites that are mainly due to uncontrolled fiber orientation during composites manufacturing can reduce the strength of the composite (Cranston and Reitz, 1980; Hatta and Yamashita, 1988). Thus, it would be very desirable to perform a solidification of the resin where the local concentration and orientation of the fibers are fully controlled. The objective of this paper is to elaborate on a mathematical model and an accompanying numerical algorithm that are capable of simulating fully three-dimensional ferromagnetic fluid flow (representing the resin and the suspended nickel-coated fibers) and solidification under the influence of an arbitrarily distributed and oriented external magnetic field. The basic idea is that the coated fibers will align with the local magnetic lines of force, which are different from streamlines. The pattern of these lines depends on the flow field and the variation of the externally applied magnetic field.

During a controlled solidification process (Dulikravich and Hayes, 1988), it is very important to understand fully the process of solid phase formation. The accumulated solid phase effectively reduces and deforms the cross-sectional area of the passages and causes significant local variations in pressure and flow field shear stresses. During the solidification or melting process, secondary flows are generated due to strong thermal buoyancy forces. These processes can be controlled in the case of strong heat transfer if influenced by a global body force.

One such body force is the general electromagnetic Lorentz force, which is created in any electrically conducting fluid when either a magnetic field or an electric potential field is applied. It has been shown (Lee and Dulikravich, 1991a, 1991b; Lee et al., 1991a; Dulikravich et al., 1991a, 1991b; Kosovic et al., 1991; Dulikravich and Kosovic, 1992) that the magnetic field can eliminate vorticity from the flow field, while the electric field can enhance it (Lee et al., 1991b). During the curing process in composites manufacturing, we usually work with weakly electrically conducting resins. Although very poorly, they do conduct electricity because of the presence of iron atoms, salts, or acids. At the same time, if fibers are coated with a thin layer of a ferromagnetic material, the fibers will respond to the applied electromagnetic fields by rotating and translating in the melt until they become aligned with the magnetic lines of force. This principle was demonstrated experimentally (Yamashita et al., 1989; Gandhi et al., 1989) and proven for a short nickel-coated carbon fiber analytically (Hatta and Yamashita, 1988). Thus, if a relatively strong magnetic field is applied, the flow field will respond (Heiser, 1964; Ievlev and Levin, 1989; Ozoe and Okada, 1989) and the solid/liquid front shape and the velocity field could be manipulated (Vives, 1989; Dulikravich et al., 1991b; Dulikravich and Kosovic, 1992). In this work we have formulated the entire problem as time dependent and three dimensional although our computational results will be for steady two-dimensional situations only.

In this first attempt at numerically simulating the process, we have assumed that the fluid is of a Newtonian type. In reality, local orientation of the short fibers and their volumetric concentration in the resin will make physical properties of the resin–fiber mixture (viscosity, heat conductivity, specific heat, electrical conductivity, magnetic permeability, etc.) tensor quantities. Moreover, due to the magnetic field imposed, the fibers will exert higher hydrodynamic resistance to the flowing resin. These physical effects have not been incorporated in the present study since they require development of a new complex mathematical model involving mixture theory and a complete electro-magneto-hydrodynamic formulation.

Analytical Model

From Maxwell's equations and a relationship between an induced electric current, J_i, an electric field, E_i, and an ex-

Contributed by the Heat Transfer Division and presented at the National Heat Transfer Conference, San Diego, California, August 9–12, 1992. Manuscript received by the Heat Transfer Division April 1992; revision received August 1992. Keywords: Mass Transfer, Materials Processing and Manufacturing Processes, Phase-Change Phenomena. Associate Technical Editor: Y. Bayazitoglu.

ternally applied magnetic field, H_i, in a moving medium given by Ohm's law

$$J_i = \sigma(E_i + \mu\epsilon_{ijk}v_jH_k) \tag{1}$$

where σ, μ, and v_j are the coefficient of electric conductivity, coefficient of magnetic permeability, and fluid velocity vector, respectively, we can derive the magnetic field transport equation (Chandrasekhar, 1961; Pai, 1962; Stuetzer, 1962; Jeffrey, 1966; Lee and Dulikravich, 1991a) as

$$H_{i,t} - (v_jH_i - v_iH_j)_{,j} = \frac{1}{\mu\sigma}H_{i,jj} \tag{2}$$

Subscripts after the comma designate partial differentiation with respect to the variable or variables that follow the comma. The entire set of Navier-Stokes partial differential equations for the fluid flow and a set of the partial differential equations for magnetic field transport can be nondimensionalized by introducing the relations

$$v_i^* = \frac{v_i}{v_o} \quad x_i^* = \frac{x_i}{l_o} \quad t^* = \frac{tv_o}{l_o} \quad p^* = \frac{p}{\rho_o v_o^2} \tag{3}$$

$$g^* = \frac{g_i}{g} \quad H_i^* = \frac{H_i}{H_o} \quad \theta = \frac{\Delta T}{\Delta T_o} \quad e^* = \frac{e}{c_{po}\Delta T_o} \tag{4}$$

where T_c is the temperature of the cold wall and T_h is the temperature of the hot wall, so that $\Delta T = T - T_c$, and $\Delta T_o = T_h - T_c$. Here, subscript zero designates reference values, while asterisk designates nondimensional variables.

In this work only incompressible Newtonian fluid flow will be considered, while accounting for thermal buoyancy via an extended Boussinesq approximation in the form that is valid even when fluid properties vary as a function of temperature (Gray and Giorgini, 1976). Fluid density and coefficients of specific heat, viscosity, and heat conduction can be expressed as general functions of temperature (Gray and Giorgini, 1976)

$$\rho = \rho_o\rho'(\theta) \quad c_p = c_{po}c_{po}'(\theta) \tag{5}$$

$$\eta = \eta_o\eta'(\theta) \quad k = k_ok'(\theta) \tag{6}$$

where the primed values denote arbitrary functions of nondimensional temperature, θ. Here, ρ, η, c_p, and k are fluid density, coefficient of viscosity, coefficient of specific heat at constant pressure, and coefficient of thermal conductivity, respectively. The nondimensional density ρ' can be expanded in a Taylor series while retaining only the first-order term

$$\rho' = 1 - \alpha\Delta T = 1 - \alpha^*\theta \tag{7}$$

so that

$$\alpha^* = \frac{\partial\rho'}{\partial\theta} = \frac{\Delta T_o\rho_o}{\rho_o\Delta T_o}\frac{\partial\rho'}{\partial\theta} = \frac{\Delta T_o}{\rho_o}\frac{\partial\rho}{\partial T} = \Delta T_o\alpha \tag{8}$$

It can be assumed that the coefficient of thermal expansion, α, is constant in the range of temperatures that are of interest in a particular case. When the term $(\Delta T_o\alpha) \ll 1$, equations more general than what is known as Boussinesq approximation can be derived for the fluid with nonconstant properties (Gray and Giorgini, 1976). For incompressible flows $c_p = c_v$. Thus, it follows that $de = c_vdT = c_pdT$. In the case of a liquid/solid mixture the enthalpy per unit mass of the mushy region becomes

$$dh = c_pdT + LdS \tag{9}$$

where L is the latent heat (enthalpy of solid/liquid phase change) and S is the volumetric fraction of the solid phase. Then

$$v_ih_{,i} = c_pv_iT_{,i} - Lv_iS_{,i} = (c_p - LS_{,T})v_iT_{,i} \tag{10}$$

Let $c_{pe} = c_p - LS_{,T}$ be an equivalent specific heat so that

$$c_{pe} = c_{po}c_{pe}' = c_{po}\left(c_p' - \frac{LS_{,\theta}\theta_{,T}}{c_{po}}\right) \tag{11}$$

where S could be an arbitrary function of θ and c_{pe}' is the nondimensional equivalent specific heat. This approach is called the "enthalpy method" (Poirier and Salcudean, 1986). With the following nondimensional groups:

Nomenclature

c_p = specific heat at constant pressure, J kg^{-1} K^{-1}
c_v = specific heat at constant volume, J kg^{-1} K^{-1}
E = electric field, V m^{-1}
Ec = Eckert number
Fr = Froude number
g = gravity force per unit volume, m s^{-2}
Gr = Grashof number
H = magnetic field, A m^{-1}
Ht = Hartmann number
J = electric current density, A m^{-2}
k = heat conductivity coefficient, W m^{-1} K^{-1}
l = length, m
L = latent heat of liquid/solid phase change, J kg^{-1}
Mm = magnetic Mach number; Mm^2 = ReRm/Ht^2
p = pressure, kg m^{-1} s^{-2}
Pm = magnetic Prandtl number
Pr = Prandtl number
Re = hydrodynamic Reynolds number
Rm = RePm = magnetic Reynolds number
S = volume fraction of the solid phase
t = time, s
T = absolute temperature, K
ΔT_o = $T_h - T_c$ = temperature difference, K
v = (u, v, w) = velocity vector, m s^{-1}
x, y, z = Cartesian coordinates, m
α = thermal expansion coefficient, K^{-1}
β = artificial compressibility coefficient
η = coefficient of shear viscosity, kg m^{-1} s^{-1}
θ = nondimensional temperature
μ = magnetic permeability, H m^{-1}
ξ, η, ζ = nonorthogonal grid-following coordinates
ρ = density, kg m^{-3}
σ = electrical conductivity, Ω^{-1} m^{-1}
ϕ = nondimensional gravity potential
Φ = viscous dissipation function, kg m^{-1} s^{-3}

Subscripts

c = cold wall
h = hot wall
o = reference values

Superscripts

* = nondimensional values
$'$ = function of nondimensional temperature

Reynolds number $\mathrm{Re}=\dfrac{\rho_o v_o l_o}{\eta_o}$

Froude number $\mathrm{Fr}^2=\dfrac{v_o^2}{g l_o}$

Grashof number $\mathrm{Gr}=\dfrac{\rho_o^2 \alpha g l_o^3 \Delta T_o}{\eta_o^2}$

Eckert number $\mathrm{Ec}=\dfrac{v_o^2}{c_{po}\Delta T_o}$

Prandtl number $\mathrm{Pr}=\dfrac{\eta_o c_{po}}{k_o}$

Magnetic Prandtl number $\mathrm{Pm}=\dfrac{\mu\sigma\eta_o}{\rho_o}$

Hartmann number $\mathrm{Ht}=\mu l_o H_o\left(\dfrac{\sigma}{\eta_o}\right)^{1/2}$

Magnetic Reynolds number $\mathrm{Rm}=\mathrm{Re}\ \mathrm{Pm}$

Magnetic Mach number $\mathrm{Mm}^2=\dfrac{\mathrm{ReRm}}{\mathrm{Ht}^2}=\dfrac{\rho_o v_o^2}{\mu H_o^2}$

(12)

the conservation laws in nondimensional form become

$$v_{i,i}=0 \tag{13}$$

$$v_{i,t}+(v_i v_j)_{,j}=\frac{1}{\mathrm{Re}}(\eta' v_{i,j})_{,j}-\bar{p}_{,i}+\frac{\mathrm{Gr}\theta}{\mathrm{Re}^2}g_i+\frac{\mathrm{Ht}^2}{\mathrm{RmRe}}(H_{ik})_{,k} \tag{14}$$

$$\theta_{,t}+v_i\theta_{,i}=\frac{1}{\mathrm{RePr}\ c_{pe}'}(k'\theta_{,i})_{,i}+\frac{\mathrm{EcHt}^2}{\mathrm{Rm}^2\mathrm{Re}\ c_{pe}'}\epsilon_{ijk}\epsilon_{ilm}H_{k,j}H_{m,l} \tag{15}$$

$$H_{,t}-(v_jH_i-v_iH_j)_{,j}=\frac{1}{\mathrm{Rm}}H_{i,jj} \tag{16}$$

It should be pointed out that the viscous dissipation can be neglected from an order of magnitude analysis since

$$\frac{\rho_o c_{pe}\dfrac{\partial T}{\partial t}}{\Phi^{(i)}}=\frac{\mathrm{Re}}{\mathrm{Ec}}\ggg 1 \tag{17}$$

The combination of nondimensional hydrodynamic, hydrostatic, and magnetic pressures is

$$\bar{p}=p+\frac{\phi}{\mathrm{Fr}^2}+\frac{1}{\mathrm{Mm}^2}H_iH_i \tag{18}$$

where ϕ is the nondimensional gravity potential defined as $g_i = \phi_{,i}$.

Numerical Algorithm

Equations (13)–(16) represent a global system of coupled nonlinear partial differential equations. The global system has been split in two subsystems in order to simplify programming. The Navier-Stokes equations, Eqs. (13)–(15), constitute the first substystem and the magnetic field transport equations, Eq. (16), constitute the second subsystem. To integrate each subsystem, the explicit Runge-Kutta time stepping method (Jameson et al., 1981) was used in an alternating manner (Lee and Dulikravich, 1991a).

The general form of each subsystem is the same. The nondimensional three-dimensional Navier-Stokes equations for incompressible flows in conservative form expressed in generalized curvilinear nonorthogonal coordinates are

$$\frac{\partial\tilde{\mathbf{Q}}}{\partial t}+\frac{\partial\tilde{\mathbf{E}}}{\partial\xi}+\frac{\partial\tilde{\mathbf{F}}}{\partial\eta}+\frac{\partial\tilde{\mathbf{G}}}{\partial\zeta}=D^2+\tilde{\mathbf{S}} \tag{19}$$

where $\tilde{\mathbf{Q}}$ is the solution vector and $\tilde{\mathbf{E}}$, $\tilde{\mathbf{F}}$, and $\tilde{\mathbf{G}}$ are the flux vectors. The transformed source vector is denoted by $\tilde{\mathbf{S}}$. Definitions of these vectors will be given for both systems of equations (Navier-Stokes and magnetic transport) separately. For the Navier-Stokes equations, the generalized vectors are defined as

$$\tilde{\mathbf{Q}}=\frac{1}{J}\begin{bmatrix}\bar{p}/\beta\\ u\\ v\\ w\\ \theta\end{bmatrix}\quad \tilde{\mathbf{E}}=\frac{1}{J}\begin{bmatrix}U\\ Uu+\xi_{,x}\bar{p}\\ Uv+\xi_{,y}\bar{p}\\ Uw+\xi_{,z}\bar{p}\\ U\theta\end{bmatrix}\quad \tilde{\mathbf{F}}=\frac{1}{J}\begin{bmatrix}V\\ Vu+\eta_{,x}\bar{p}\\ Vv+\eta_{,y}\bar{p}\\ Vw+\eta_{,z}\bar{p}\\ V\theta\end{bmatrix}$$

$$\tilde{\mathbf{G}}=\frac{1}{J}\begin{bmatrix}W\\ Wu+\zeta_{,x}\bar{p}\\ Wv+\zeta_{,y}\bar{p}\\ Ww+\zeta_{,z}\bar{p}\\ W\theta\end{bmatrix}\quad \tilde{\mathbf{S}}=\begin{bmatrix}0\\ \tilde{d}_2\\ \tilde{d}_3\\ \tilde{d}_4\\ \tilde{d}_5\end{bmatrix}\quad \tilde{\mathbf{D}}=\frac{1}{\mathrm{Re}}\begin{bmatrix}0\\ \eta'\\ \eta'\\ \eta'\\ k'\\ \overline{\mathrm{Pr}c_p'}\end{bmatrix}T \tag{20}$$

where $J = \partial(\xi, \eta, \zeta)/\partial(x, y, z)$ is the Jacobian determination of the geometric transformation from physical Cartesian coordinates x, y, z into ξ, η, ζ computational space.

The system of equations given by Eqs. (13)–(16) is not hyperbolic since there is no physical time derivative term in the mass conservation equation. Consequently, the system cannot be integrated simultaneously. In order to integrate the system simultaneously and obtain a steady-state solution, an artificial compressibility (Chorin, 1967) term, $\partial/\partial t(\bar{p}/\beta J)$, has been added to the mass conservation equation, Eq. (13). Here, β is an artificial compressibility coefficient, a user-specified parameter that depends on the problem geometry, grid, flow parameters, etc. (Lee and Dulikravich, 1991c). In the steady-state limit the artificial compressibility term tends to zero. Thus, it does not influence the steady-state solution.

The source vector $\tilde{\mathbf{S}}$ contains the influence of the ponderomotive force due to the magnetic field and the thermal buoyancy force. Its components are given as

$$\tilde{d}_2=\frac{\mathrm{Ht}^2}{\mathrm{RmRe}}\left(\frac{\partial}{\partial\xi}\left(\frac{\hat{H}_\xi H_x}{J}\right)+\frac{\partial}{\partial\eta}\left(\frac{\hat{H}_\eta H_y}{J}\right)+\frac{\partial}{\partial\zeta}\left(\frac{\hat{H}_\zeta H_z}{J}\right)\right)+\frac{\mathrm{Gr}\theta}{\mathrm{Re}^2 J}g_x \tag{21}$$

$$\tilde{d}_3=\frac{\mathrm{Ht}^2}{\mathrm{RmRe}}\left(\frac{\partial}{\partial\xi}\left(\frac{\hat{H}_\xi H_y}{J}\right)+\frac{\partial}{\partial\eta}\left(\frac{\hat{H}_\eta H_y}{J}\right)+\frac{\partial}{\partial\zeta}\left(\frac{\hat{H}_\zeta H_y}{J}\right)\right)+\frac{\mathrm{Gr}\theta}{\mathrm{Re}^2 J}g_y \tag{22}$$

$$\tilde{d}_4=\frac{\mathrm{Ht}^2}{\mathrm{RmRe}}\left(\frac{\partial}{\partial\xi}\left(\frac{\hat{H}_\xi H_z}{J}\right)+\frac{\partial}{\partial\eta}\left(\frac{\hat{H}_\eta H_z}{J}\right)+\frac{\partial}{\partial\zeta}\left(\frac{\hat{H}_\zeta H_z}{J}\right)\right)+\frac{\mathrm{Gr}\theta}{\mathrm{Re}^2 J}g_z \tag{23}$$

$$\tilde{d}_5=\frac{1}{c_{pe}'}\frac{\mathrm{EcHt}^2 J}{\mathrm{RmRe}^2}\left(\tilde{P}_1^2+\tilde{P}_2^2+\tilde{P}_3^2\right) \tag{24}$$

where H_x, H_y, H_z are the components of the magnetic field vector in Cartesian coordinates, g_x, g_y, g_z are components of the unit vector in the direction of gravity force, and

$$\tilde{P}_1=\frac{\partial}{\partial\xi}\left(\frac{H_z\xi_{,y}-H_y\xi_{,z}}{J}\right)+\frac{\partial}{\partial\eta}\left(\frac{H_z\eta_{,y}-H_y\eta_{,z}}{J}\right)+\frac{\partial}{\partial\zeta}\left(\frac{H_z\zeta_{,y}-H_y\zeta_{,z}}{J}\right) \tag{25}$$

$$\tilde{P}_2=\frac{\partial}{\partial\xi}\left(\frac{H_x\xi_{,z}-H_z\xi_{,x}}{J}\right)+\frac{\partial}{\partial\eta}\left(\frac{H_x\eta_{,z}-H_z\eta_{,x}}{J}\right)+\frac{\partial}{\partial\zeta}\left(\frac{H_x\zeta_{,z}-H_z\zeta_{,x}}{J}\right) \tag{26}$$

Table 1 Nondimensional numbers

Passage	Closed	Straight	U-shaped	Arbitrary
Melt	(silicon)	(undefined)	(undefined)	(saline)
Gr	56.769×10^6	0.0	0.0	0.0
Re	8300	100	20	234.44
Ec	7.869×10^{-8}	1	1	6.46×10^{-8}
Pr	0.0116	7.9	7.9	36.9
Pm	4.44×10^{-6}	1	1	2.68×10^{-3}
Ht	$209.3 B_o$ or $2093 B_o$	5 or 10	5 or 10	0.0 or $0.5027 B_o$

$$\tilde{P}_3 = \frac{\partial}{\partial \xi}\left(\frac{H_y \xi_{,x} - H_x \xi_{,y}}{J}\right) + \frac{\partial}{\partial \eta}\left(\frac{H_y \eta_{,x} - H_x \eta_{,y}}{J}\right) + \frac{\partial}{\partial \zeta}\left(\frac{H_y \zeta_{,x} - H_x \zeta_{,y}}{J}\right) \tag{27}$$

The diffusion term in general curvilinear coordinates is

$$D^2 = \left(\frac{\tilde{\mathbf{D}}}{J} g_{ij} (J\tilde{\mathbf{Q}})_{,j}\right)_{,i} \tag{28}$$

The metric tensor is defined as

$$g_{ij} = \frac{\partial \bar{x}_i}{\partial \hat{x}_j} \frac{\partial \bar{x}_j}{\partial \hat{x}_i} \tag{29}$$

where $\bar{x}_i$ is the Cartesian coordinate vector and $\hat{x}_i$ is the curvilinear coordinate vector:

$$\bar{x}_i = (x, y, z)^T \qquad \hat{x}_i = (\xi, \eta, \zeta)^T \tag{30}$$

Here, the superscript T represents a transpose. The contravariant components U, V, W of the velocity vector are related to the velocity components u, v, w in the Cartesian system as follows:

$$\begin{bmatrix} U \\ V \\ W \end{bmatrix} = \begin{bmatrix} \xi_{,x} & \xi_{,y} & \xi_{,z} \\ \eta_{,x} & \eta_{,y} & \eta_{,z} \\ \zeta_{,x} & \zeta_{,y} & \zeta_{,z} \end{bmatrix} \begin{bmatrix} u \\ v \\ w \end{bmatrix} \tag{31}$$

Similarly, the contravariant components $\hat{H}_\xi$, $\hat{H}_\eta$, $\hat{H}_\zeta$ of the magnetic field vector are defined as

$$\begin{bmatrix} \hat{H}_\xi \\ \hat{H}_\eta \\ \hat{H}_\zeta \end{bmatrix} = \begin{bmatrix} \xi_{,x} & \xi_{,y} & \xi_{,z} \\ \eta_{,x} & \eta_{,y} & \eta_{,z} \\ \zeta_{,x} & \zeta_{,y} & \zeta_{,z} \end{bmatrix} \begin{bmatrix} H_x \\ H_y \\ H_z \end{bmatrix} \tag{32}$$

For the subsystem containing the magnetic field transport equations, the solution vector $\tilde{\mathbf{Q}}$, the flux vectors $\tilde{\mathbf{E}}$, $\tilde{\mathbf{F}}$, $\tilde{\mathbf{G}}$, and the source vector $\tilde{\mathbf{S}}$ are

$$\tilde{\mathbf{Q}} = \frac{1}{J}\begin{bmatrix} H_x \\ H_y \\ H_z \end{bmatrix} \quad \tilde{\mathbf{E}} = \frac{1}{J}\begin{bmatrix} H_x U - u\hat{H}_\xi \\ H_y U - v\hat{H}_\xi \\ H_z U - w\hat{H}_\xi \end{bmatrix} \quad \tilde{\mathbf{F}} = \frac{1}{J}\begin{bmatrix} H_x V - u\hat{H}_\eta \\ H_y V - v\hat{H}_\eta \\ H_z V - w\hat{H}_\eta \end{bmatrix}$$

$$\tilde{\mathbf{G}} = \frac{1}{J}\begin{bmatrix} H_x W - u\hat{H}_\zeta \\ H_y W - v\hat{H}_\zeta \\ H_z W - w\hat{H}_\zeta \end{bmatrix} \quad \tilde{\mathbf{S}} = 0 \quad \tilde{\mathbf{D}} = \frac{1}{\mathrm{Rm}}\mathbf{I} \tag{33}$$

In the case of three-dimensional magnetohydrodynamics, the system of eight partial differential equations needs to be solved by integrating intermittently a subsystem of five fluid flow equations and a subsystem of three magnetic field transport equations and transferring the information through the sourcelike terms (Lee, 1990; Lee and Dulikravich, 1991a). The explicit Runge-Kutta time-stepping algorithm and finite difference scheme with artificial compressibility (Chorin, 1967) were used in the general nonorthogonal curvilinear boundary conforming coordinate system. The pressure boundary condition at the solid walls of the passages was enforced using a normal momentum equation, instead of the boundary layer approximation that the normal pressure gradient at the solid boundary is zero. Inlet and exit boundary conditions were treated using the method of characteristics (Lee and Dulikravich, 1991a). The explicit time integration scheme was used because it can be efficiently vectorized and because additional equations can be easily added to the system. The rate of convergence of explicit schemes is generally much lower than for implicit schemes, but when fully vectorized, these schemes need less central processor unit time to reach convergence than implicit schemes. This advantage of explicit schemes is more pronounced when three-dimensional problems with complex geometries are studied.

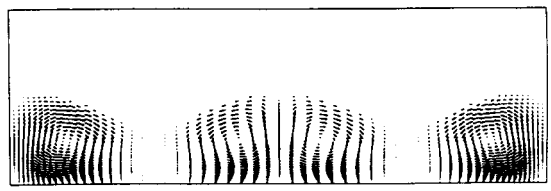

Fig. 1(*a*) Velocity vector field

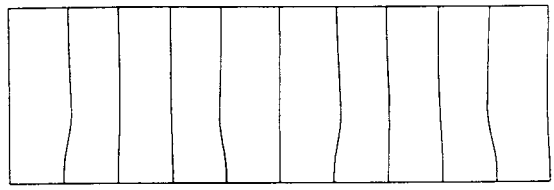

Fig. 1(*b*) Magnetic lines of force

Fig. 1 Closed container with a weak constant magnetic field

Computational Results

A computer code written in Fortran was developed for simulation of two-dimensional solidification processes under the influence of a steady externally applied magnetic field. Four configurations were tested numerically: a closed container cooled uniformly from above, a straight channel flow with nonuniformly cooled top and bottom walls, a U-shaped channel with nonuniformly cooled inner and outer walls, and an arbitrarily shaped channel nonuniformly cooled from top and the bottom. Nondimensional parameters used in the calculations are summarized in Table 1.

Closed Container. Mathematical and numerical models for solidification of a fluid flow were first tested in the case of a closed rectangular container of aspect ratio 3:1. It was discretized with 60 × 60 grid cells that were clustered toward the four walls. Vertical walls were thermally insulated, while the top wall had a uniform undercooling nondimensional temperature of $\theta = -10$. At the same time, the bottom wall had a uniform nondimensional temperature of $\theta = 1$. A uniform magnetic field of Ht = 209.3 B_o was applied vertically downward. We have specified $B_o = 1$ Tesla. The resulting velocity vector field (Fig. 1*a*) indicates strong recirculation of the melt due to thermal buoyancy. The solid accrued is visible toward the top wall. The resulting magnetic force lines (lines that are locally tangent to the magnetic force vector) are depicted in Fig. 1(*b*), indicating that the fluid motion has distorted the magnetic force lines. Notice that the magnetic force lines along which the short fibers would align have an entirely different pattern from the flow field streamlines.

When a stronger magnetic field (Ht = 2093 B_o) was applied, the thermal buoyancy flow was significantly suppressed (Fig.

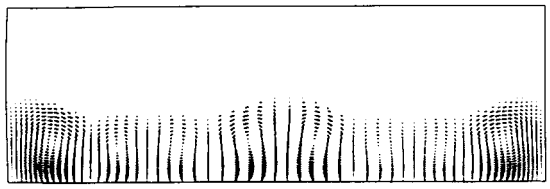

Fig. 2(*a*) Velocity vector field

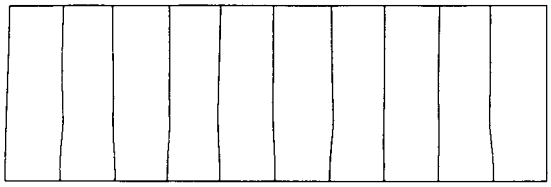

Fig. 2(*b*) Magnetic lines of force

Fig. 2 Closed container with a strong constant magnetic field

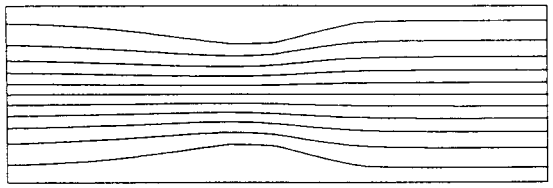

Fig. 3(*a*) Streamlines

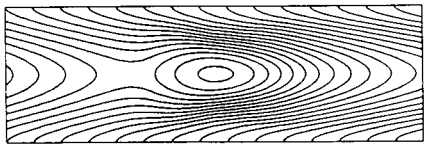

Fig. 3(*b*) Magnetic lines of force

Fig. 3 Straight channel with a weak constant magnetic field

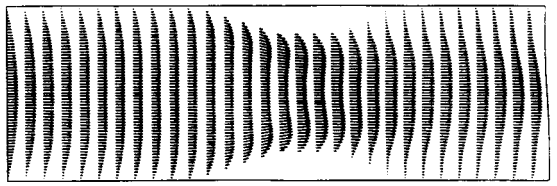

Fig. 4(*a*) Velocity vector field

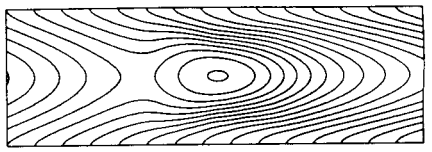

Fig. 4(*b*) Magnetic lines of force

Fig. 4 Straight channel with a strong constant magnetic field

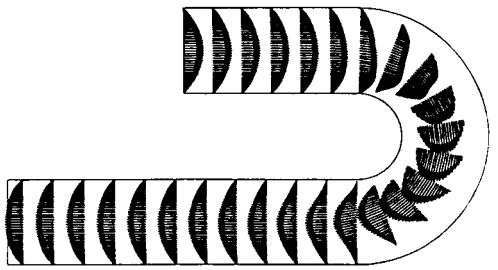

Fig. 5(*a*) Velocity vector field

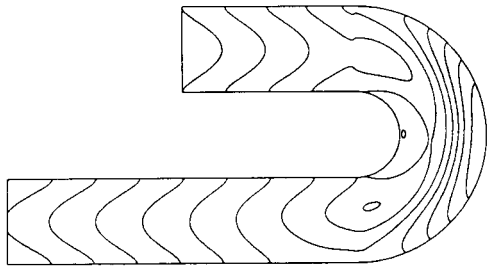

Fig. 5(*b*) Magnetic lines of force

Fig. 5 U-shaped channel with a weak constant magnetic field

2*a*) and the magnetic force lines straightened somewhat (Fig. 2*b*). The amount of solid accrued at the top wall is smaller than with Ht = 209.3 B_o.

Straight Channel. The second configuration studied was a straight two-dimensional channel of aspect ratio 3:1 with the flow direction from left to right (Fig. 3*a*). A uniform nondimensional temperature $\theta = 1$ was imposed at the inlet. Along the walls a smoothly varying cooling was specified as $\theta = 1 - 11 \sin(\pi x/3)$. Both velocity components were specified at the inlet, while a combination of hydrostatic, hydromagnetic and hydrodynamic pressure was specified at the exit. Properties of the fluid flow were defined by the nondimensional numbers, which are given in Table 1. All physical properties were assumed not to vary with temperature. The flow field was discretized with 60 × 60 nonclustered grid cells.

The first test case represents a solidifying flow field with an imposed uniform magnetic field of Ht = 5 acting vertically downward. The computed streamlines (Fig. 3*a*) clearly outline the solidified zones attached to the channel walls. Computed lines of magnetic force are given in Fig. 3(*b*), indicating that they have been strongly affected by the flow field. Notice how different the two patterns are. Magnetized fibers will align themselves according to the pattern in Fig. 3(*b*).

To test the influence of a stronger magnetic field on solidification, a test run was performed with the viscosity varying linearly in the mushy region and a vertically downward pointing constant magnetic field of Ht = 10. The computed velocity vector field (Fig. 4*a*) and the magnetic lines of force (Fig. 4*b*) demonstrate that the magnetic field is affected even further by the flow field. The presence of a magnetic field in an already existing mean flow inhibits the growth of the solid layers because of the higher speed of the fluid next to the solid/fluid interface. This is typical for magnetohydrodynamics.

U-Shaped Channel. The next test configuration represented a solidifying flow in a U-shaped channel of constant width where the fluid enters at the upper end and exits at the lower end. The same type of boundary condition was imposed on inlet temperature and velocity as in the case of a straight channel. Along the straight parts of the walls the temperature was kept constant ($\theta = 1$). Along the curved parts of the walls the nondimensional temperature varied according to $\theta = 1 - 11 \sin(\pi/2 - \omega)$ where ω is the angle between the wall point and the horizontal. The computational grid had 264 × 60 cells that were clustered toward the walls. Nondimensional numbers used with the U-shaped channel are given in Table 1.

In the first test case a uniform magnetic field (Ht = 5) was applied perpendicular to the walls of the entire U-shaped channel. The computed velocity vector field (Fig. 5*a*) demonstrates that the magnetic field effectively eliminates flow recirculation regions. The predicted magnetic force lines (Fig. 5*b*) are significantly distorted from the straight-line pattern that would connect inner and outer walls if there would be no flow through the channel.

In the second test case a stronger magnetic field (Ht = 10)

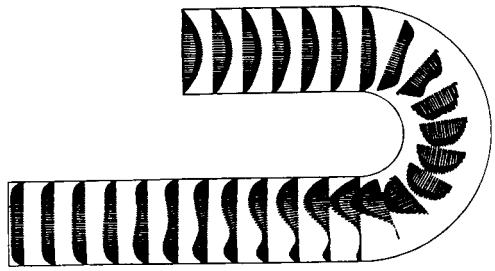

Fig. 6(*a*) Velocity vector field

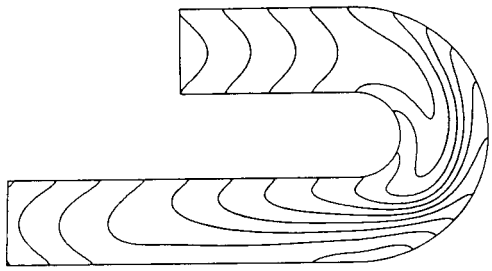

Fig. 6(*b*) Magnetic lines of force

Fig. 6 U-shaped channel with a strong constant magnetic field

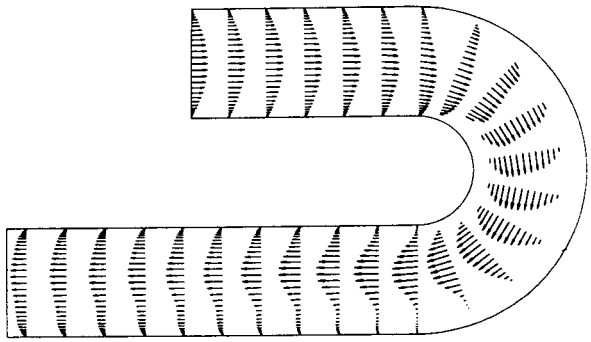

Fig. 7(*a*) Velocity vector field

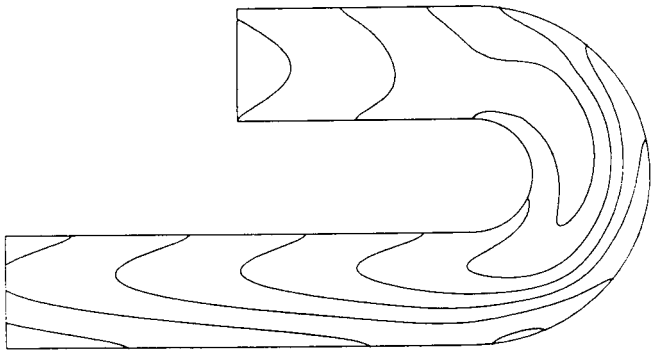

Fig. 7(*b*) Magnetic lines of force

Fig. 7 U-shaped channel with a variable magnetic field

was applied in the same manner, resulting in a dramatic change in the flow pattern (Fig. 6*a*). Plots of the magnetic lines of force (Fig. 6*b*) demonstrate their complex pattern that could be exploited to position and orient short ferromagnetically coated fibers in the flow field and, consequently, in the solidified layers.

In the case that the externally applied magnetic field is not uniform, but instead varies along the curved parts of the channel walls according to Ht = 10 − 5 sin (π/2-ω), the flow field pattern (Fig. 7*a*) and the magnetic lines of force (Fig. 7*b*) will

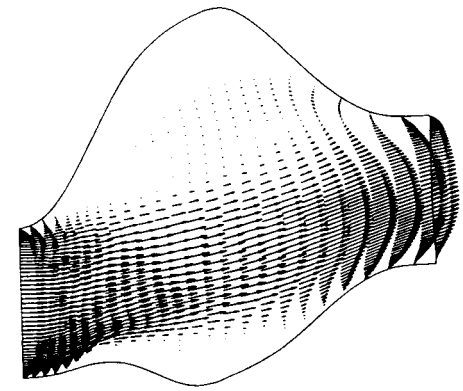

Fig. 8(*a*) Velocity vector field

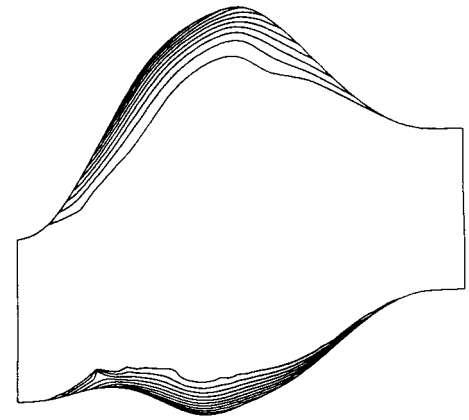

Fig. 8(*b*) Isotherms

Fig. 8 Arbitrary passage without magnetic field

be considerably different. This clearly demonstrates the conceptual feasibility of controlling not only the orientation, but also the concentration of the fibers in the resin during the curing process.

Arbitrary Channel. Finally, the mathematical model and the computer code were tested using a set of physical flow parameters corresponding to a saline solution flow in an arbitrary shaped channel with undercooled walls. As in the case of channel flow, the temperature of the walls from inlet to exit was varying according to a sinusoidal distribution $\theta = 1 - 11 \sin(\pi i / i\max)$ where i is the grid cell index in the x direction ($1 < i < i\max$). Fluid temperature at the inlet was a uniform $T = 283$ K corresponding to $\theta = 1$ since $T_h = 283$ K and $T_c = 273$ K so that $\Delta T_o = T_h - T_c = 10$ K. This made the coldest point on the wall have a temperature of −100°C. In the case when a steady uniform magnetic field was applied, it acted vertically downward between the inlet and 80 percent of the channel length, while no magnetic field was applied over the remaining 20 percent of the channel length. The characteristic quantities that were used for nondimensionalization are: $c_{po} = c_{po\,\mathrm{liq}}$, $k_o = k_{o\,\mathrm{liq}}$, $l_o = 0.01$ m, $v_o = 0.1$ m/s. Since the value for the magnetic permeability could not be found in the open literature, we have arbitrarily assumed it to be $\mu = 50\,\mu_v$, where $\mu_v = 4\pi \times 10^{-7}$ is the magnetic permeability for vacuum. If $B_0 = \mu_v H_0$, the remaining terms in the equation for Ht can be grouped so that Ht is directly proportional to B_0, which is measured in Teslas. For example, if Ht = 0.5 B_0 and the value for B_0 is 10, this means that the Hartmann number Ht = 5 can be achieved with the magnetic field of 10 T.

The nonorthogonal boundary-conforming computational grid consisted of 100 × 58 grid cells that were clustered toward the inlet and the passage top and bottom walls. The grid was

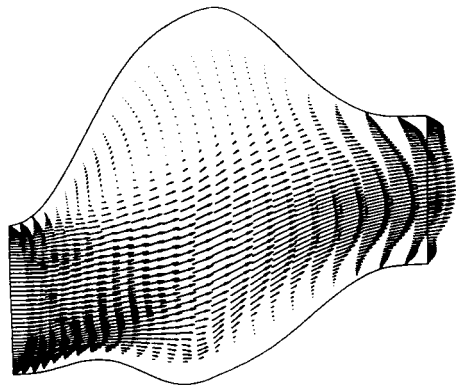

Fig. 9(*a*) Velocity vector field

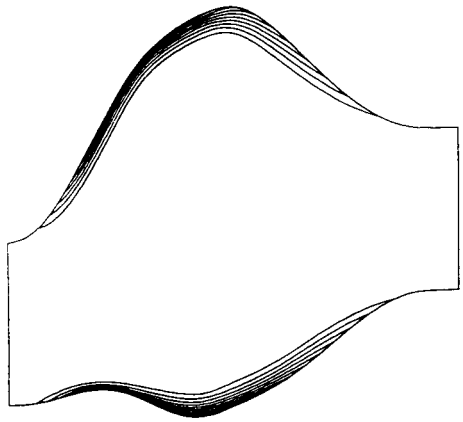

Fig. 9(*b*) Isotherms

Fig. 9 Arbitrary passage with a constant magnetic field

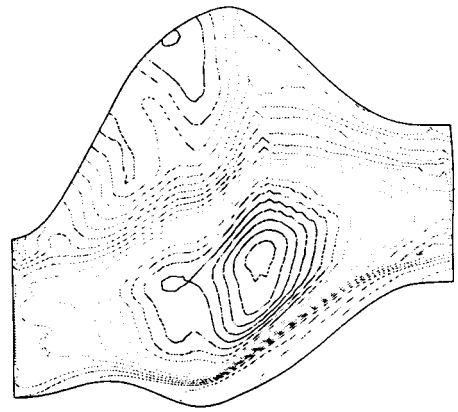

Fig. 10(*a*) Magnetic lines of force

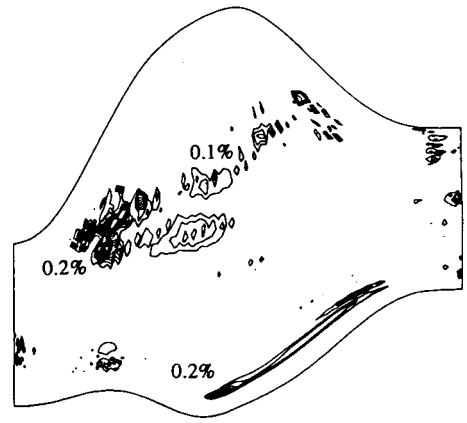

Fig. 10(*b*) Joule heating contours

Fig. 10 Arbitrary passage with a constant magnetic field

generated using our grid optimization algorithm (Kennon and Dulikravich, 1986).

A comparison of the computational results with and without an external magnetic field shows that the velocity profiles change under the influence of the magnetic field due to the ponderomotive force (Figs. 8*a* and 9*a*). More importantly, the solidified layers in the case where no external magnetic field was applied are thicker and differently shaped compared to the freezing with the magnetic field as indicated by the isotherms in the solid phase without (Fig. 8*b*) and with (Fig. 9*b*) the magnetic field. A very complex pattern of magnetic lines of force (Fig. 10*a*) clearly indicates that the coated short fibers could be manipulated using appropriately distributed magnetic field strength along the boundaries of the domain. It should be pointed out that it is the higher speed of the fluid close to the solid/liquid interface that decreases the residence time of the fluid particles in the mushy region, thus decreasing the rate of solid accretion. This increase in the fluid speed in the boundary layer regions is caused by the presence of the magnetic field. On the other hand, Joule heating (Fig. 10*b*) would have a profound influence on the solidification rate in the case of a lower electrical conductivity of the fluid and in flows generated purely by thermal buoyancy.

Conclusions

An analytical and a numerical formulation have been developed for the theoretical prediction of solidification processes in fluid flows inside undercooled passages with and without the influence of an externally applied steady magnetic field. Computational results confirm that the magnetic field has a profound influence on the solidifying flow field since it eliminates flow recirculation regions and causes distorted velocity profiles having pronounced overshoots close to the solid boundaries. The temperature field also changes under the influence of the external magnetic field. This change influences heat transfer through the boundaries and consequently the amount of the solid phase accrued on undercooled walls. Specifically, the influence of the ponderomotive force and, to a much lesser extent, Joule heating are such that they tend to reduce the amount of the accrued solid phase. Combined with the predicted complex patterns of the magnetic field force lines, this indicates a possibility for the development of a computational inverse design/optimization algorithm capable of achieving desired configurations of the solidified layers and desired distribution and orientation of magnetized short fibers within the solidified layers.

Acknowledgments

All computations were performed remotely on the Cray-YMP computer at NASA Ames Research Center NAS facility and at Cray Research, Inc. in Eagan, Minnesota and post-processed at Penn State on equipment donated by Apple Computer, Inc. The authors are thankful to the reviewers for useful comments and to Mr. Scott G. Sheffer for correcting the grammar in this paper.

References

Balasubramaniam, T. A., and Bowman, H. F., 1977, "Thermal Conductivity and Thermal Diffusivity of Biomaterials: A Simultaneous Measurement Technique," *Journal of Biomedical Engineering*, Aug., pp. 148-154.

Chandrasekhar, S., 1961, *Hydrodynamic and Hydromagnetic Stability*, Dover Publication Inc., New York.

Chorin, A. J., 1967, "A Numerical Method for Solving Incompressible Viscous Flow Problems," *Journal of Computational Physics*, Vol. 2, pp. 12-26.

Cranston, J. J., and Reitz, J. A., III, 1980, "SMC Molding Techniques for

Optimized Mechanical Properties in Structural Applications," *Polymer and Plastics Technology and Engineering*, Vol. 15, pp. 97–114.

Diller, K. R., 1985, "The Influence of Controlled Ice Nucleation on Regulating the Thermal History During Freezing," *Cryobiology*, Vol. 22, pp. 268–281.

Dulikravich, G. S., and Hayes, L. J., 1988, "Control of Surface Temperatures to Optimize Survival in Cryopreservation," in: *Symposium on Computational Methods in Bioengineering*, R. L. Spilker and B. R. Simon, eds., ASME BED-Vol. 9, pp. 255–265.

Dulikravich, G. S., Kosovic, B., and Lee, S., 1991a, "Solidification of Variable Property Melts in Closed Containers: Magnetic Field Effects," *Proc. 13th IMACS World Congress on Computation and Applied Math.*, Dublin, Ireland, July 22–26.

Dulikravich, G. S., Kosovic, B., and Lee, S., 1991b, "Solidification in Reduced Gravity With Magnetic Fields and Temperature-Dependent Physical Properties," in: *Symposium on Heat and Mass Transfer in Solidification Processes*, G. S. Advani and C. Beckerman, eds., ASME HTD-Vol. 175/MD-Vol. 25, pp. 61–73.

Dulikravich, G. S., and Kosovic, B., 1992, "Solidification of Variable Property Melts Under the Influence of Low Gravity, Magnetic Fields and Electric Fields," AIAA Paper No. 92-0694.

Fazzio, R. G., and Jacobs, H. R., 1974, "Heat Transfer Coefficients of Blood in Small Tubes and Capillaries," *AIChE Symposium Series 138*, Vol. 70, pp. 233–240.

Gandhi, M. V., Thompson, B. S., and Choi, S. B., 1989, "A New Generation of Innovative Ultra-advanced Intelligent Composite Materials Featuring Electro-Rheological Fluids: An Experimental Investigation," *Journal of Composite Materials*, Vol. 23, Dec., pp. 1232–1255.

Gray, D. D., and Giorgini, A., 1976, "The Validity of the Boussinesq Approximation for Liquids and Gases," *International Journal of Heat and Mass Transfer*, Vol. 19, pp. 545–551.

Hatta, H., and Yamashita, S., 1988, "Fiber Orientation Control by Means of Magnetic Moment," *Journal of Composite Materials*, Vol. 22, May, pp. 484–500.

Heiser, W. H., 1964, "Influence of Magnetic Fields Upon Separation," *AIAA Journal*, Vol. 2, No. 12, pp. 2217–2218.

Ievlev, V. M., and Levin, V. B., 1989, "Laminarization of a Submerged Jet of Electrically Conducting Fluid by Means of a Longitudinal Magnetic Field," *Izvestia Akademii Nauk SSSR, Mekhanika Zhidkosti i Gaza*, No. 6, Nov.–Dec., pp. 35–40.

Jameson, A., Schmidt, W., and Turkel, E., 1981, "Numerical Solution of the Euler Equations by Finite Volume Methods Using Runge-Kutta Time-Stepping Scheme," AIAA Paper No. 81-1259.

Jeffrey, A., 1966, *Magnetohydrodynamics*, University Mathematical Texts 33, Oliver & Royd Ltd., Edinburgh, United Kingdom.

Kennon, S. R., and Dulikravich, G. S., 1986, "Optimization of Computational Grids," *AIAA Journal*, Vol. 24, No. 7, pp. 1069–1073.

Kosovic, B., Dulikravich, G. S., and Lee, S., 1991, "Freezing Under the Influence of a Magnetic Field: Computer Simulation," *Proceedings of 1991 ICHMT Int. Symposium on Heat and Mass Transfer in Biomedical Engineering*, K. Diller, A. Shitzer, and S. Sideman, eds., Athens, Greece, Sept. 2–6.

Kosovic, B., and Dulikravich, G. S., 1992, "Unsteady Solidification in Microgravity," *Symposium on Topics in Heat Transfer*, Vol. 3, ASME HTD-Vol. 206-3, pp. 13–20.

Lee, S., and Dulikravich, G. S., 1991a, "Magnetohydrodynamic Steady Flow Computations in Three Dimensions," AIAA Paper No. 91-0388; also in *International Journal for Numerical Methods in Fluids*, Vol. 13, No. 8, Oct., pp. 917–936.

Lee, S., and Dulikravich, G. S., 1991b, "Computation of Magnetohydrodynamic Flow With Joule Heating and Buoyancy," *Proceedings of International Aerospace Congress*, Melbourne, Australia, May.

Lee, S., and Dulikravich, G. S., 1991c, "Performance Analysis of DMR Method for Acceleration of Iterative Algorithms," AIAA Paper No. 91-0241.

Lee, S., Dulikravich, G. S., and Kosovic, B., 1991a, "Interaction of a Magnetic Field With Blood Flow," *Proceedings of 17th Annual Northeast Bioengineering Conference*, University of Connecticut, Hartford, CT, Apr. 4–5.

Lee, S., Dulikravich, G. S., and Kosovic, B., 1991b, "Electrohydrodynamic (EHD) Flow Modeling and Computations," AIAA Paper No. 91-1469.

Ozoe, H., and Okada, K., 1989, "The Effect of the Direction of the External Magnetic Field on the Three-Dimensional Natural Convection in a Cubical Enclosure," *International Journal of Heat and Mass Transfer*, Vol. 32, No. 2, pp. 1939–1954.

Pai, S.-I., 1962, *Magnetogasdynamics and Plasma Dynamics*, Springer Verlag, Vienna.

Poirier, D., and Salcudean, M., 1986, "On Numerical Methods Used in Mathematical Modeling of Phase Change in Liquid Metals," ASME Paper No. 86-WA/HT-22.

Stuetzer, O. M., 1962, "Magnetohydrodynamics and Electrohydrodynamics," *The Physics of Fluids*, Vol. 5, No. 5, pp. 534–544.

Sud, V. K., Sekhon, G. S., and Mishra, R. K., 1977, "Pumping Action of Blood by a Magnetic Field," *Bulletin of Mathematical Biology*, Vol. 39, pp. 385–390.

Vives, C., 1989, "Effects of a Magnetically Forced Convection During the Crystallization in Mould of Aluminum Alloys," *Journal of Crystal Growth*, Vol. 94, pp. 739–750.

Yamashita, S., Hatta, H., Sugano, T., and Murayama, K., 1989, "Fiber Orientation Control of Short Fiber Composites: Experiment," *Journal of Composite Materials*, Vol. 23, pp. 32–41.